Available online at www.sciencedirect.com
SCIENCE DIRECT
Journal of Power Sources 152 (2005) 210–217
JOURNAL OF POWER SOURCES
www.elsevier.com/locate/jpowsour

Short communication

Electrical coupling in proton exchange membrane fuel cell stacks☆

G.-S. Kim [a], J. St-Pierre [a,*], K. Promislow [b], B. Wetton [c]

[a] *Ballard Power Systems, Inc., 4343 North Fraser Way, Burnaby, BC V5J 5J9, Canada*
[b] *Michigan State University, Department of Mathematics, East Lansing, MI 48824, USA*
[c] *University of British Columbia, Department of Mathematics, 1984 Mathematics Road, Vancouver, BC V6T 1Z2, Canada*

Received 27 January 2005; accepted 27 January 2005
Available online 9 March 2005

Abstract

Stack models require consideration of interactions between cells owing to practical variation of cell model parameters and different location/environment in the stack leading to thermal, electrical and mass transfer gradients. A previously developed voltage/current distribution model (electrical interaction) was extended and validated using two types of anomalies (bus plate material change, partially inactive cell located at the stack center), two anomaly locations and one or two anomalies within the stack. A measurement method for the principal cell interaction damping factor is discussed which can be used to easily and approximately predict the number of cells that are impacted by an anomaly.

Keywords: Polymer electrolyte fuel cell; Stack; Model; Voltage/current distribution; Cell anomaly

1. Introduction

The development of proton exchange membrane fuel cells for automotive, stationary and portable electrical power has received considerable attention in recent years. Computational design tools have kept pace with these advances, ranging from simple algebraic equations to fully coupled mass and thermal transport in three dimensions [1]. These models strive to describe all significant processes affecting the performance of a unit cell including electrical/electrochemical phenomena, which offer significant cost savings in terms of testing and design cycle time.

Fuel cells generally comprise an assembly of single cells. These single cells are not identical from a manufacturing standpoint or have a different location/environment in the stack which can lead to performance inequalities during operation resulting in thermal, electrical (via shared bipolar plates) and mass transfer gradients between cells, and therefore in cell interactions or coupling. This terminology is preferred, for example, over the more common term of current/voltage distribution to emphasize the potential 'infection' of healthy cells located near an anomalous cell. Cell interaction is an important model feature, for example, to define manufacturing tolerances for cell components, to accurately predict stack behavior or to assess series reliability. Most fuel cell stack models do not completely address interactions between cells and little information is available. From this standpoint, reactant flow distribution was briefly discussed [2] and, a stack model including temperature and prescribed reactant flow distributions was derived for a solid oxide fuel cell [3].

A first attempt was made to evaluate the character and importance of these effects for thermal interactions in proton exchange membrane fuel cells with particular emphasis on simplicity to achieve rapid computational convergence [4,5]. More recently, a similar electrical interaction model was developed for the same application including an efficient numerical method to solve the nonlinear coupled system [6,7]. Validation of the full model and an asymptotic solution are presented here. The unit cells are described by simple, steady-state, 1 + 1-dimensional models appropriate for straight reac-

☆ This paper was presented at the 2004 Fuel Cell Seminar, San Antonio, TX, USA.

* Corresponding author. Tel.: +1 604 412 3186; fax: +1 604 453 3782.
E-mail address: jean.st-pierre@ballard.com (J. St-Pierre).

0378-7753/$ – see front matter © 2005 Elsevier B.V. All rights reserved.
doi:10.1016/j.jpowsour.2005.01.029

Nomenclature

A	summation term coefficient
c_1	dimensionless membrane/electrode assembly resistivity
C_O	flow field channel oxygen concentration
C_{ref}	oxygen reference concentration
C_ε	computational parameter
E_0	open-circuit voltage
F	Faraday constant
G	cell interaction damping factor
G_1	principal cell interaction damping factor
i	through-plane current density
$\tilde{i}$	dimensionless through-plane current density perturbation
i_0	exchange current density
i_*	transition current density
I	in-plane length specific current
j	cell number
J	number of cells impacted by an anomaly
k	interaction term detection limit
L_t	bipolar plate thickness
n	summation parameter
r^2	correlation coefficient
R	gas constant
R_t	membrane/electrode assembly ohmic resistance
T	temperature
V	cell voltage
$\tilde{V}$	dimensionless cell voltage perturbation
W	parameter (Wagner number analog)
x	flow field channel coordinate
$\tilde{x}$	dimensionless flow field channel coordinate

Greek symbols

α_c	cathode reaction charge transfer coefficient
δ	mass transfer coefficient
λ	bipolar plate length-specific resistivity
λ_b	bus plate length-specific resistivity
λ_e	end plate length-specific resistivity
λ_*	dimensionless bipolar plate resistivity
ρ_s	bipolar plate volume-specific resistivity

tant gas channel designs. The linear, asymptotic version of the model is used to give analytic insight into the effect of the coupling, including estimates of the coupling extent in terms of the number of adjacent cells affected.

2. Model summary

The core model element is the previously developed unit cell model [8] simplified and extended by a more detailed description of current/voltage distribution within bipolar and end plates. The main model assumptions are:

- Straight channel design;
- High fuel cell aspect ratio motivates consideration of a 1 + 1-dimensional model (along the flow field channel, through the membrane) with averaged quantities over the channel-to-channel direction;
- Catalyst layers have zero thickness;
- Linear temperature profile between cell inlet and outlet;
- Reactant streams obey the ideal gas law;
- Reactant streams are transported by convection with a common average velocity;
- Reactant streams are saturated with water vapor;
- Anode kinetics are neglected;
- Water vapor condensation immediately occurs upon reaching over-saturation conditions;
- Liquid water presence in reactant flow field channels and gas diffusion electrodes is neglected;
- Membrane hydration and its relationship to conductivity is neglected;
- Membrane water crossover from one compartment to the other is neglected.

Some of these assumptions lead to a convenient model reduction avoiding the iterative process associated with reactant counter-flow operation and resulting in faster computation (removal of membrane and anode dependencies). A modified Butler–Volmer relationship is used:

$$V = E_0 - iR_t - \frac{RT}{F\alpha_c}\ln\frac{iC_{ref}}{i_0(C_O - \delta i)} \quad (1)$$

Eq. (1) was further extended to relax the constraint $i < C_O/\delta$ for computational reasons by introducing $i_* = (C_O - C_\varepsilon)/\delta$. Eq. (1) is used for $i < i_*$, whereas Eq. (2) is used for $i \geq i_*$:

$$V = E_0 - i_*R_t - \frac{RT}{F\alpha_c}\ln\frac{i_*C_{ref}}{i_0C_\varepsilon} - \left(R_t + \frac{RT}{F\alpha_c}\left(\frac{1}{i_*} + \frac{\delta}{C_\varepsilon}\right)\right)(i - i_*) \quad (2)$$

This simple unit cell model was found to satisfactorily represent experimental data obtained for different oxidant stoichiometries [8]. In a stack environment, where individual cells can be subjected to different operating conditions, the local current density values can be different leading to in-plane bipolar plate currents. The unknown voltage for each cell, denoted by $V^j(x)$, is derived by local current (through-plane current density i, in-plane length specific current I) and voltage balances (Fig. 1):

$$\frac{dI^{j/j+1}(x)}{dx} = i^j(x) - i^{j+1}(x) \quad (3)$$

$$\frac{dV^j(x)}{dx} = \lambda(I^{j-1/j}(x) - I^{j/j+1}(x)) \quad (4)$$

where $\lambda = \rho_s/L_t$ represents the length-specific resistivity of the bipolar plate. Differentiation of Eq. (4) and using (3) leads

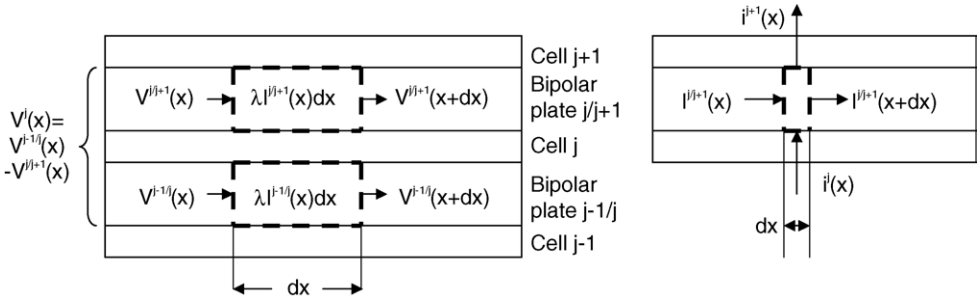

Fig. 1. Bipolar plate voltage (left) and current balances (right).

to the fundamental voltage equation for electrical interactions between cells:

$$\frac{\mathrm{d}^2 V^j(x)}{\mathrm{d}x^2} - \lambda(i^{j-1}(x) - 2i^j(x) + i^{j+1}(x)) = 0 \tag{5}$$

The equation set (5) is solved using Eqs. (1) and (2), and boundary conditions (zero in-plane currents at inlet and outlet) and modifications to voltage and current balances at the end plates (bus plate and its connection, electrically insulating plates inserted after the bus plates). The channel oxygen concentrations change with consumption and so are determined non-locally by the local current densities $i^j(x)$. These oxygen concentrations in turn affect the voltage balance Eq. (1) and so represent non-local coupling in the voltage equations.

Linear analysis of the model equations leads to analytical solutions for the through-plane current disturbance including a cell interaction damping factor useful to define the number of cells impacted by an anomaly:

$$\tilde{i}^j(\tilde{x}) = \sum_{n=1}^{\infty} A_n G_n^{|j|} \cos(n\pi\tilde{x}) \tag{6}$$

$$G_n = \frac{2 + n^2\pi^2 W - \sqrt{(2 + n^2\pi^2 W)^2 - 4}}{2}, \quad W = \frac{c_1}{\lambda_*} \tag{7}$$

where W represents an analog to the Wagner number [9] and is the ratio of the dimensionless resistivity of the membrane/electrode assembly c_1 and λ_*, a dimensionless bipolar plate resistivity. The principal cell interaction damping factor G_1 tends to 1 when W tends to 0 (bipolar plate effect dominates with resulting strong coupling), whereas G_1 tends to 0 when W tends to ∞ (cell resistance effect dominates with resulting weak coupling).

If it is assumed that the cell voltage is located within the ohmic regime and the principal interaction parameter controls the behavior, Eq. (6) leads to the cell voltage perturbation:

$$\tilde{V}^j(\tilde{x}) \approx R_t A_1 G_1^j \cos(\pi\tilde{x}) \tag{8}$$

The cell voltage perturbation difference between two locations is therefore:

$$\log(\tilde{V}^j(\tilde{x}_1) - \tilde{V}^j(\tilde{x}_0)) \approx \log(R_t A_1(\cos(\pi\tilde{x}_1) - \cos(\pi\tilde{x}_0))) + j\log G_1 \tag{9}$$

Therefore, a plot of the left hand side of Eq. (9) versus j would provide an experimental measurement of the principal cell interaction parameter that can be compared to the Eq. (7) estimate. An estimate of the number of cells impacted by an anomaly can also be derived from Eq. (6) by determining for which j value the term G_1^j decays to a predetermined value k:

$$J = \frac{\log k}{\log G_1} \tag{10}$$

Some minor modifications were made to the model to take account of the different cell performance obtained during the validation tests, to implement the specific anomaly type investigated and to account for the presence of a bipolar plate located besides the bus plates. The c_1 and λ_* parameter values were changed, to take account of polarization curve and bus plate material differences between this work and earlier results [7], from respectively 0.150 (c_1) and 19 (λ_*) to 0.335 and 9.5. These changes reflect kinetic, ohmic and mass transport modifications. As a result, the principal cell interaction damping factor G_1 computed from Eq. (7) has changed from 0.76 [6] to 0.83 (Table 1). Such a high value indicates a potential for strong electrical interactions between cells.

Table 1
Summary of the principal cell interaction damping factor values and other related parameters

	Experimental (15-cell stack)			Full model				Eq. (7)
	100 A	200 A	300 A	15-cell stack			100-Cell stack (300 A)	
				100 A	200 A	300 A		
G_1	0.80	0.83	0.79	0.65	0.64	0.61	0.72	0.83
r^2	0.65	0.86	0.75	0.968	0.954	0.978	0.978	–
J	6	10	10	5	6	7	9	–
k	0.262	0.155	0.095	0.116	0.069	0.031	0.050	–

A partially inactive cell was selected as an anomaly located within a stack. In this case, the through-plane current density is invariably equal to 0 over part of the active area (1/3 was selected). The current balance needs to be modified and the $i^j(x)$ term is eliminated (Fig. 1). As a result the derivation used for Eq. (5) leads to:

$$\frac{d^2V^j(x)}{dx^2} - \lambda(i^{j-1}(x) + i^{j+1}(x)) = 0, \quad x \leq \frac{L}{3} \tag{11}$$

Since the local through-plane current density is equal to 0, iterative computations cannot be performed using this variable. Rather, the iterative formulation based on the voltage variable was used (more details about the voltage and current iterative formulations are provided in [6]). One of the end cells bipolar plates is adjacent to a bus plate. Therefore, in-plane currents can circulate in either plate (parallel arrangement) depending on the relative resistivity of each material. The end plate resistivity was therefore defined as:

$$\frac{1}{\lambda_e} = \frac{1}{\lambda_b} + \frac{1}{\lambda} \tag{12}$$

3. Experimental

A 15-cell Mk 902 stack with the hydrogen stream in counter-flow to both coolant and air streams was used (in this context, the cell inlet indicated in Fig. 2a corresponds to both air and coolant inlets). The operating conditions were selected to minimize the presence of other types of cell interaction (thermal interaction, flow distribution). This was achieved using sufficiently large air stoichiometries (3.64, 1.78, 1.82, 1.58 for respective currents of 100, 150, 200, 300 A) and by selecting the approach used to create an anomaly. More specifically, the use of larger stoichiometries for smaller currents is justified to maintain a sufficient reactant flow rate circulating in each cell and consequently to ensure a uniform flow distribution. Other operating conditions were (air/H_2): 67/70 °C dew points, 3.04/3.04 bara, 70 °C coolant inlet temperature with a coolant flow rate set to achieve a temperature rise of 10 °C, 1.53 fuel stoichiometry. In addition, the electrical anomaly size introduced within the stack was selected to maximize the observable effect. Two types of anomalies were considered (Fig. 2); stainless steel replacing copper as the bus plate material (respective resistivity values of 7.4×10^{-7} and 1.7×10^{-8} Ω m), inactive section near the inlet of the middle cell 8 (1/3 of its active area length). It should be emphasized that these specific selections may not necessarily be representative of the anomalies that are observed. For example, whereas local inactive areas can develop as a result of degradation, an error in the bus plate material is significantly less likely to occur in practice. However, the anomalies investigated were selected because they were easy to implement and provided opportunities to test model validity beyond the required range of interest. The active area reduction was achieved by covering the membrane/electrode assembly with a Kapton™ film on both the cathode and anode sides (high temperature resistance polymer impermeable to oxygen) resulting in an expected current density increase of 1.5 in the remainder of cell 8.

For each operating condition, voltage measurements were simultaneously performed for all cells at several locations along the flow field direction (straight channel design [10]) and all within the active area (inlet, middle, outlet). The bus plate connection locations are also indicated in Fig. 2. As an indication of the absence of other types of cell interaction, baseline voltage measurements were also completed for all cells (two Cu bus plates, no inactive section for any of the cells) yielding standard deviations of respectively 3–5, 6–10, 5–6 and 8–12 mV at 100, 150, 200 and 300 A (Fig. 3).

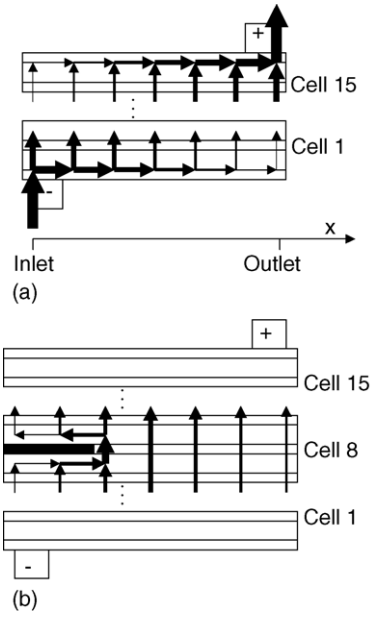

Fig. 2. Schematic cell configuration and current redistribution as a result of (a) resistive bus plate material and (b) inactive cell area. The inlet and outlet locations refer to both air and coolant streams.

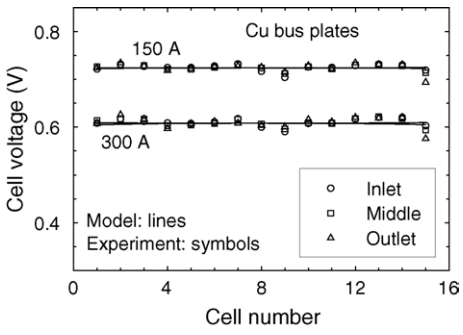

Fig. 3. Comparison between stack voltage distribution measurements and model computations for the case of two copper bus plates.

4. Results and discussion

Fig. 3 illustrates a comparison between the model predictions and experimental data in the absence of anomalies. It is observed that the model can adequately predict stack performance for a normal operating cell. More specifically, the current bus plate design leads to negligible end cell effects even at 300 A. The voltage is constant along the cell length especially for the cells located near the bus plates.

Fig. 2a illustrates the resistive bus plate case (stainless steel). At the negative bus plate, the current cannot easily circulate along its length resulting in a significant voltage drop. As a result, the through-plane current density for the first cell decreases towards the cell outlet leading to a larger cell voltage. This situation is reversed at the positive bus plate leading to lower current densities near the cell inlet and hence higher cell voltages. For cells located between the end cells, bipolar plates allow current to redistribute due to the existence of voltage gradients between cell inlet and outlet. As a result, the size of the voltage difference between cell inlet and outlet decreases away from the bus plates. Copper bus plates being more conductive do not lead to such disturbances since current circulates more easily with little voltage drop (Cu/Cu and Cu/stainless steel bus plates combinations) resulting in more even current distribution and little cell voltage difference between cell inlet and outlet.

Fig. 2b illustrates the inactive inlet cell area case. For this case, the current is forced to circulate along the bipolar plate length on both sides of the inactive area. For adjacent cells, the situation is similar to the Fig. 2a case. As a result, the cell voltage near the inlet is high (low current density) but lower near the middle and outlet sections of the cells. This effect decreases away from the anomaly due to current redistribution in the bipolar plates. As for the anomalous cell, the voltage is lowest near the middle (highest current density region) and almost unaffected near the cell outlet. As for the anomalous cell inlet, the cell voltage is low. The origin of this low voltage is not electrochemical (the cell is inactive) but rather due to in-plane current circulation leading to a voltage decrease on one side of the anomalous cell and a voltage increase on the other side. The net effect is a decrease in cell voltage, which in extreme cases can lead to cell voltage reversal (see Figs. 6c and 7).

It was found that for each of the Fig. 2 cases discussed, the model reproduces the shape as well as the magnitude of the disturbance effect without the need to refit the model parameters (beyond the modifications discussed in the model summary section) for a significant range of current density. Fig. 4 illustrates a comparison between experimental data and model predictions for the case of two stainless steel bus plates whereas Fig. 5 illustrates a similar comparison for the case of one copper and one stainless steel bus plate, and Fig. 6 shows the comparison for the case of a partially inactive cell. The most significant discrepancy occurs in a region where the largest current densities are predicted (middle cell voltage near the interface between the inactive and active sections

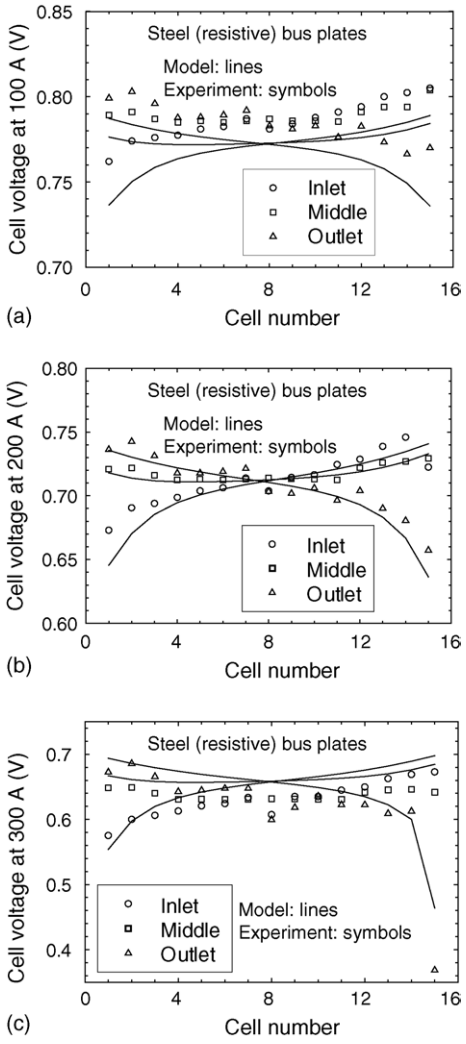

Fig. 4. Comparison between stack voltage distribution measurements and model computations for the case of two stainless steel bus plates: (a) 100 A, (b) 200 A and (c) 300 A.

for cell 8 in Fig. 6). At this position, the local current density can reach values up to 1.8 A cm^{-2} (200 A total current) with an associated large local voltage gradient [7] spread over an extended region (approximately one-third of the active area length). A small voltage measurement location change, corresponding to ~7% of the active area length, was found to be sufficient to almost eliminate this discrepancy (Fig. 7). All the experimental results of Figs 4–6 and the corresponding model predictions are illustrated in Fig. 8, demonstrating a significantly high degree of correlation ($r^2 = 0.988$) and model predictive capability.

The validity of Eq. (9) was investigated by considering the experimental and modeling results of Fig. 5, which shows the stainless steel bus plate perturbation decay until it virtually disappears (model curves converge to the same voltage value towards the negative bus plate/cell 1 direction). In addition, Eq. (9) was derived with the objective to maximize the value of an observable (using only one cell voltage value at a given location would not have been as sensitive). Fig. 9 illustrates

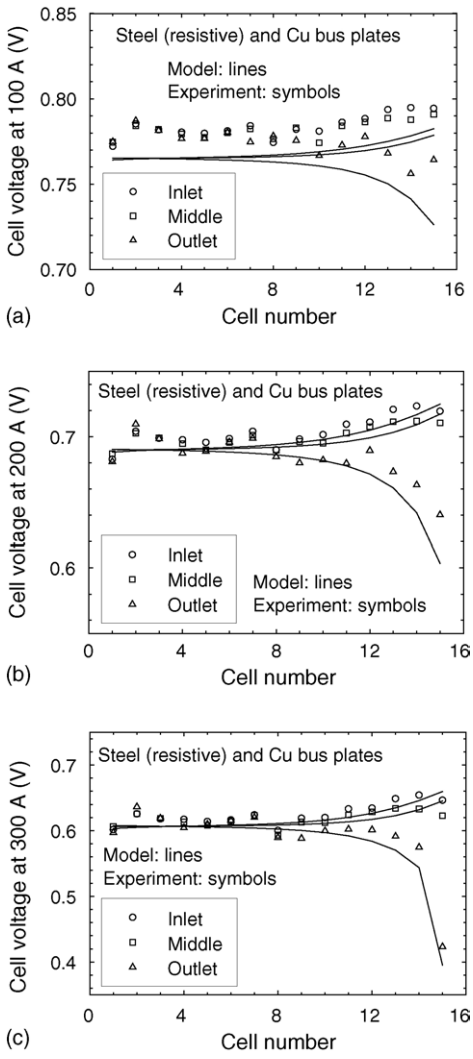

Fig. 5. Comparison between stack voltage distribution measurements and model computations for the case of one stainless steel bus plate and one copper bus plate: (a) 100 A, (b) 200 A and (c) 300 A.

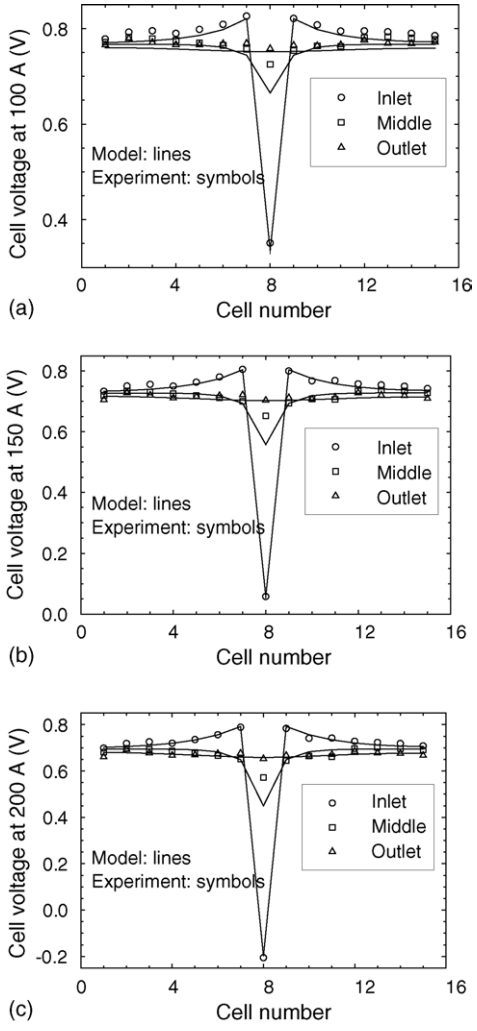

Fig. 6. Comparison between stack voltage distribution measurements and model computations for the case of a partially inactive cell 8 near the inlet area: (a) 100 A, (b) 150 A and (c) 200 A.

the results for the 300 A case (cell numbering was reversed for convenience) and Table 1 summarizes the principal cell interaction damping factor values for all three current densities. It is observed that both experimental data and full model computations follow Eq. (9) but to different degrees as evidenced by the different regression coefficient values (Table 1). Better agreement is found for the model than for the experimental data. This may be attributed to experimental error and small number of data points used for correlation. Experimental voltage differences lower than 10 mV were ignored since this approximately corresponded to the standard deviation reported in Section 3. The G_1 value derived from the model data is significantly different from the value derived from Eq. (7). This difference is ascribed to the assumption made to derive Eq. (7). Only the main term in Eq. (6) was retained ($n = 1$), which implies that all the other terms have some impact while maintaining the semi-log character of Eq. (9). More importantly, there is a significant difference between experimental and model G_1 values. As already mentioned, this is likely due to experimental error. Another possibility is to consider that the asymptotic solution was derived for an anomaly located within a stack rather than at one of its end. Still another pos-

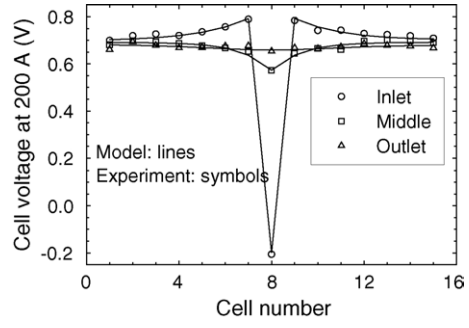

Fig. 7. Comparison between stack voltage distribution measurements and model computations for the case of a partially inactive cell 8 near the inlet area and 200 A. Cell voltage measurement location for the middle cell case was modified by a value equivalent to ∼7% of the active area length.

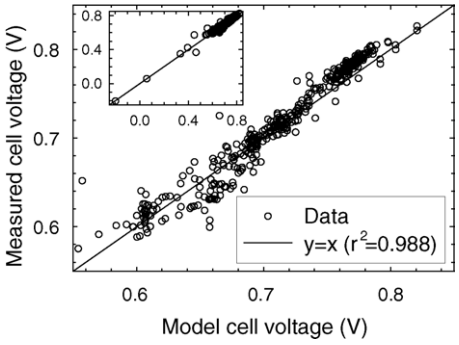

Fig. 8. Comparison between all stack voltage distribution measurements (Figs. 4–6) and model computations (Figs. 4–6).

sibility is the disrupting presence of other anomalies (see last paragraph of Section 4). More data and analysis are required to resolve this discrepancy. This is particularly important to easily predict the number of cells impacted by an anomaly Eq. (10), which requires a G_1 and a k estimate. A k estimate is obtained from Eq. (10) by determining the number of cells at the intersection of Eq. (9) fits (Fig. 9) with the 0.01 ordinate value (10 mV represents the assumed detection limit based on the observed standard deviation) and using the corresponding G_1 value. Results appear in Table 1 and indicate that 0.1 represents an achievable value of k within the present setup and measurement accuracy. The number of cells impacted by an anomaly varies from 5 to 10 and, model and experimental estimates roughly agree with each other.

By comparison, the number of cells impacted by a thermal anomaly is less and ranges from 2 to 3 for the same stack design and similar operating conditions [4,5]. The difference suggests that an independent evaluation is required to properly account for different effects during stack design activities. The difference also provides additional support to the small impact of this particular interaction on the experimental results.

Computations were performed with a larger stack to verify whether or not the proximity of both stack ends has an effect on cell interaction, to gain a better understanding of computational requirements and to investigate the effect of an anomaly size which was not experimentally considered

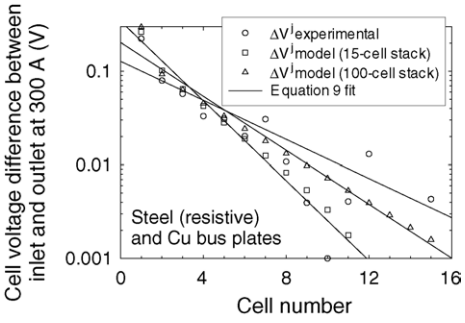

Fig. 9. Comparison between cell inlet and outlet voltage difference measurements and model computations for the case of one stainless steel bus plate and one copper bus plate, and 300 A.

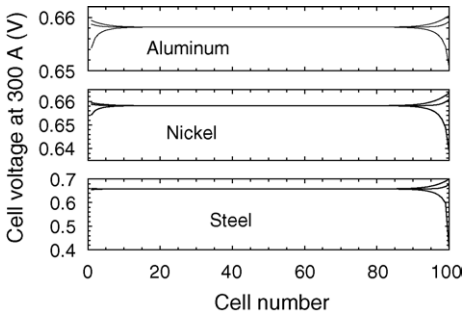

Fig. 10. 100-Cell stack voltage distribution model computations for the case of one anomalous bus plate (either stainless steel, nickel or aluminum) and one copper bus plate at 300 A. Model curves correspond to inlet, middle and outlet locations.

(only anomaly location, type and quantity were considered). A 100-cell stack was chosen with the same configuration as used for the Fig. 5 results (positive bus plate material change) using different bus plate materials of the same thickness as copper (stainless steel; nickel, $6.8 \times 10^{-8}\,\Omega\,m$; aluminum, $2.7 \times 10^{-8}\,\Omega\,m$) and a flow field channel discretized to 32 grid points. Convergence was obtained in 280 s with a 2.66 GHz Pentium 4 microcomputer equipped with 767 MB of RAM. For comparison, similar computations required 4.4 s for a 15-cell stack. The Fig. 10 results show a similar behavior as illustrated in Fig. 5. It does appear that the number of cells impacted by an anomaly does not depend on the anomaly size. This observation is not experimentally valid as the detection sensitivity is not infinite (order of 10 mV), which may result in an apparent anomaly size effect. Furthermore, a closer look revealed small differences due to the different stack size as illustrated in Fig. 9. The number of cells impacted by the anomaly has increased from 7 to 9 (Table 1). This is due to interactions between anomalies. In the 100-cell stack, the anomaly is still present after 16 cells (~1 mV, Fig. 9), which can lead to a significant in-plane current in a bipolar plate (~0.02 A). Consequently, the two bus plates in a 15-cell stack can interact although this may not be detectable. The model is useful to properly size a stack for single anomaly studies requiring cell interaction minimization.

5. Conclusion

An electrical interaction model was developed for proton exchange membrane fuel cell stacks and was validated using two types of anomalies (bus plate material change, partially inactive cell located within a stack), two locations and different quantities of anomalies (one or two). The resulting predictive capability can be used to accelerate fuel cell stack design iterations and reduce the number of experimental tests needed for design validation thereby saving significant resources. Furthermore, the approximate validity of an asymptotic solution was demonstrated leading to a potential method to measure the principal cell interaction damping factor. The asymptotic solution also led to a simple expression to esti-

mate the number of cells impacted by an anomaly (first-order estimate). Additional work is also required to further validate the cell anomaly propagation distance estimation method.

Acknowledgements

The authors acknowledge the financial support of MITACS NCE, NSERC, NSF and Ballard Power Systems, Inc.

References

[1] K.Z. Yao, K. Karan, K.B. McAuley, P. Oosthuizen, B. Peppley, T. Xie, Fuel Cells 4 (2004) 3–29.
[2] R.J. Kee, P. Korada, K. Walters, M. Pavol, J. Power Sources 109 (2002) 148–159.
[3] A.C. Burt, I.B. Celik, R.S. Gemmen, A.V. Smirnov, J. Power Sources 126 (2004) 76–87.
[4] B. Wetton, K. Promislow, A. Çağlar, in: R.K. Shah, S.G. Kandlikar (Eds.), Fuel Cell Science, Engineering and Technology, ASME, New York, NY, 2004, pp. 151–155.
[5] K. Promislow, B. Wetton, J. Power Sources, in press.
[6] P. Berg, A. Çağlar, K. Promislow, J. St-Pierre, B. Wetton, IMA J. Appl. Math., submitted for publication.
[7] P. Berg, A. Çağlar, K. Promislow, B. Wetton, J. St-Pierre, G.-S. Kim, in: 2004 Fuel Cell Seminar Abstracts, Courtesy Associates, Washington, DC, 2004.
[8] P. Berg, K. Promislow, J. St-Pierre, J. Stumper, B. Wetton, J. Electrochem. Soc. 151 (2004) A341–A353.
[9] K. Scott, Electrochemical Reaction Engineering, Academic Press, London, 1991, pp. 420–421.
[10] P.R. Gibb, International Patent Application WO 00/41260 (2000).